Proceedings of the 2001 IEEE
International Conference on Robotics & Automation
Seoul, Korea - May 21-26, 2001

An experimental undulating-fin device using the Parallel Bellows Actuator

Michael Sfakiotakis[†] David M. Lane[†] Bruce C. Davies[§]

[†]Ocean Systems Laboratory, Heriot-Watt University
Edinburgh EH14 4AS, SCOTLAND
e-mail: sfakios@cee.hw.ac.uk D.M.Lane@hw.ac.uk

[§]Department of Mechanical & Chemical Engineering, Heriot-Watt University
e-mail: B.J.Davies@hw.ac.uk

Abstract— **To investigate undulating median fin propulsion and its potential for implementation in man-made underwater vehicles, a "fin actuator" has been developed. The device consists of eight Parallel Bellows Actuators ("fin rays") arranged in a series and interconnected via a flexible material ("fin membrane"). The PBAs are pneumatically driven and allow for bending movements in any orientation plane. Position data are provided by flexible electrogoniometers. The forces generated from the fin actuator undulations are measured by a pair of tri-axial force sensors. Initial testing has concentrated on two-dimensional fin ray motions, whereby each PBA moves laterally, with the deflection angle performing a sinusoidal variation. Preliminary measurements, for a range of the propulsive waveform parameters, demonstrate reversible thrust generation and good agreement with the theoretical predictions of a momentum-based model.**

Keywords - biomimetics, gymnotiform, underwater vehicle propulsion, elongated body theory, flexible actuator.

I. Introduction

Most fish generate thrust by bending their bodies into a backward-moving propulsive wave that extends to its caudal fin (BCF locomotion). Other fish have developed alternative swimming mechanisms, involving the use of their median and pectoral fins, termed Median and/or Paired Fin (MPF) locomotion. An estimated 15% of the fish families use these modes as their routine propulsive means, while a much greater number that typically rely on BCF modes for propulsion employ MPF modes for maneuvering and stabilisation [1]. *Undulatory* motions involve the passage of a wave along the propulsive structure, while in *oscillatory* motions the propulsive structure swivels on its base without exhibiting a wave formation. Both types of motion result from the coupled oscillations of smaller elements that constitute the propulsor (i.e. muscle segments and fin rays for BCF and MPF propulsion respectively) and should be considered as a continuum [2]. Biomimetic designs for underwater vehicles have adopted two main routes, largely outlined by the BCF/MPF classification: the first includes devices that emulate the continuously flexing fish bodies for increased propulsive efficiency [3] [4], while the second category includes biologically-inspired appendages, developed mainly to improve the maneuverability of existing underwater vehicles [5] [6]. To study undulatory MPF swimming, we have developed the "fin actuator", an experimental device based on the structure of teleost fins, that utilises the Parallel Bellows Actuator (PBA) as "fin ray" units.

submitted to the *IEEE International Conference on Robotics and Automation (ICRA 2001)*, COEX, Seoul, Korea, May 21-26, 2001.

II. Biological Background

Three modes utilising median fin undulations are identified: *amiiform*, *gymnotiform* and *balistiform*. These correspond to propulsion by undulation of the dorsal, ventral and both dorsal and ventral fins, respectively. They are all highly maneuverable animals, able to swim as well backwards as they do forwards, by reversing the direction of waveform propagation on their propulsor fin. Their body is held straight during swimming, although it is flexible and

capable of undulations. This has been related to the absence of the enhanced friction drag (compared to that of the rigid body) that results from body undulations [7]. For balistiform swimmers, the existence of two main fin propulsors enables more complicated undulation schemes, e.g. passing waves at opposing directions during hovering [8]. In *rajiform* mode, found in rays and skates, swimming is by undulations of their greatly enlarged and highly flexible pectorals.

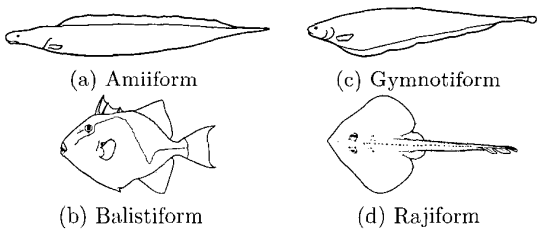

Figure 1 – Fish using undulating MPF modes.

III. Mathematical Analysis

According to the qualitative description by Breder and Edgerton [9], the thrust produced by an undulating fin is analysed into a force $\vec{F}_z$ normal to the fin base (from the simple oscillation of the fin rays) and a force $\vec{F}_x$ parallel to the fin base (resulting from the passage of the wave along the fin). There is experimental evidence to support this vector analysis [10]. Elaborate maneuvering can be achieved by varying the relative magnitude of $\vec{F}_z$ and $\vec{F}_x$, to vector the resulting force. Both physical (variations in the inter-distance, length and flexibility of fin rays) and behavioristic (amplitude, wavelength and phase differences along the fin) factors to perform this are identified in [9]. Three main approaches have been developed since to estimate the thrust and/or efficiency of undulating fin propulsion: actuator-disc method [11], elongated body theory (ebt) [7] and waving plate theory extended by blade element analysis [12]. The first is based on a simple "black box" method, while the other two attempt to provide insights on the effect of the propulsive wave parameters, as well as on the effect of fin-body interactions (in ebt) and wing shape (in extended waving plate theory). Application to MPF locomotion of the recent wake theories developed for undulatory BCF propulsion [3] presents an interesting field of research, that along with flow visualisation experiments could determine whether vorticity control mechanisms are employed by fish swimming in these modes.

IV. The Parallel Bellows Actuator

The PBA is a simple, compact and lightweight mechanism which contains no moving parts, and yet can generate motion with three degrees of freedom. Operation relies on the elastic deformation of cylindrical bellows with corrugated walls, placed at equal intervals about a central axis and constrained by end plates. Both the direction and magnitude of tip movement can be controlled. The PBA has been successfully applied to the development of dextrous end-effectors, multi-section inspection systems and walking robots [13]. Being easily depth- and pressure-compensated, it is well suited to underwater applications [14].

The input vector of bellows pressures $\mathbf{P}_{\text{in}}$ is

$$\mathbf{P}_{\text{in}} = \begin{bmatrix} P_1 \\ P_2 \\ P_3 \end{bmatrix} = \mathbf{P}_{\text{offset}} + \mathbf{P}_{\text{diff}}$$

where the number subscript identifies the pressure going into the corresponding bellows (Figure 2). $\mathbf{P}_{\text{offset}}$ is the vector of the offset pressures. If the maximum pressure available for actuation is $P_{\max}$, the maximum range of movement is obtained for

$$\mathbf{P}_{\text{offset}} = \frac{1}{2}\mathbf{P}_{\max}$$

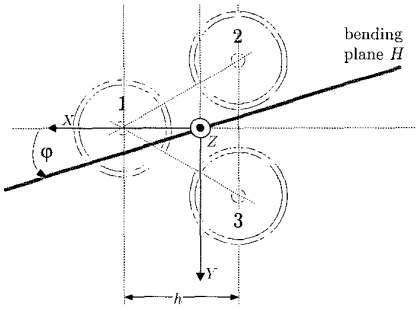

Figure 2 – Schematic of the Parallel Bellows Actuator, illustrating the bending plane H.

Assuming that the bellows material is homogenous and isotropic, and that all bellows have the same area, the orientation angle φ of the bending plane is only a function of $\mathbf{P}_{\text{in}}$. For non-zero pressure differential, the relation is [15]

$$\varphi = \arctan\left(\sqrt{3}\frac{P_3 - P_2}{2P_1 - P_2 - P_3}\right)$$

The direction and amount of movement generated in the PBA structure is controlled by the differential pressure vector $\mathbf{P}_{\text{diff}}$ appearing in Equation ??, obtained as

$$\mathbf{P}_{\text{diff}} = \Delta P \begin{bmatrix} \cos(\pi + \varphi) \\ \cos\left(\frac{5}{8}\pi + \varphi\right) \\ \cos\left(\frac{7}{3}\pi + \varphi\right) \end{bmatrix},$$

where ΔP is the magnitude of bellows pressure variation from $\mathbf{P}_{\text{mean}}$ and provides a measure of the extend of the actuator bending, which is a function of its physical properties (length and axial spring rate of the bellows, bending stiffness etc.). Their effect has been investigated largely in [15] and can be determined more accurately for a particular PBA by calibration tests. For $\Delta P = 0$ the PBA assumes its straight position.

The PBA design utilised as a fin ray in the fin actuator has an active span of $b = 0.32\,\text{m}$. Actuation is provided by a 6 bar pneumatic source, coupled to three proportional valves, adjusting the input pressures. The deflected actuator is modelled as a curve of constant radius. The main assembly parts are illustrated in Figure 3.

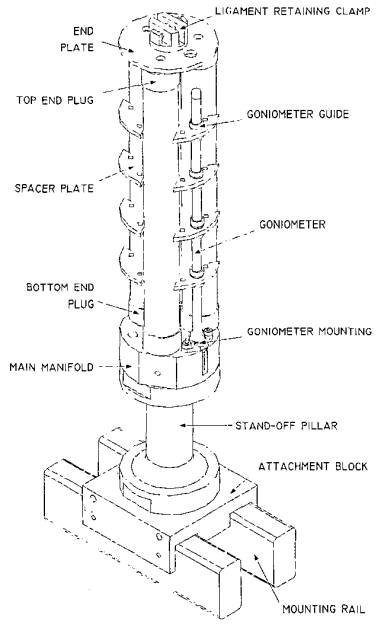

Figure 3 – Fin ray assembly indicating main components.

V. Position Sensor

Continuum devices, including the PBA, present a novel control problem in that the entire structure undergoes elastic deformation with no joints to control or measure. The use of a flexible electrogoniometer to provide position data in the form of angular displacements, was proposed during the fin actuator design.

The biplanar flexible electrogoniometer is essentially a composite wire, with two pairs of strain gauges mounted around its circumference. Because the sensor has been almost exclusively targeted at the biomedical community, it hasn't made its way into robotics, where a number of applications could benefit from its features. Disadvantages, at least in its current form, include the delicate construction and reported drift problems. Since the PBA is a flexible actuator, assuming curves similar to the preferred ones for the electrogoniometer, the sensor appears to be well suited for use in a measurement system and even for feedback in closed-loop control schemes.

We next summarise the working principle of the electrogoniometer, based on the detailed description in [16]. The reference frames used by the authors are shown in Figure 4. If the distal end is positioned so that Z_1, X_1, Z_2, X_2 axes all lie in the same plane (Figure 4), then if the goniometer is moved away from the "stretched straight" position, strain gauges SG3 and SG4 do not change their length, while SG1 and SG2 do. It can then be shown that the output of channel A is proportional to $\hat{\alpha}_y$ (the angle between X_1 and X_2), while the output of channel B is zero. A similar situation occurs when the distal end is placed so that the Z_1, Y_1, Z_2, Y_2 axes are in the same plane. Therefore, if the rotation around axis Y_1 is $\hat{\alpha}_y$ and the rotation around X_1 is $\hat{\alpha}_x$, the readings of the two goniometer channels (RCHA and RCHB) will be:

Motion plane	RCHA	RCHB
Z_1X_1	$s_A\hat{\alpha}_y$	0
Z_2X_2	0	$s_B\hat{\alpha}_x$

where s_A and s_B are the sensitivities of the two measurement channels. If the goniometer lies in a plane H rotated around Z_1 by an angle $\hat{\varphi}$, the measuring cable is *not* twisted if both X_1 and X_2 intersect the plane with the same angle $\hat{\varphi}$. In this case, the goniometer reads the projection of the flexion angle $\hat{\alpha}$ (the angle between Z_1 and Z_2) onto the planes Z_1X_1 and Z_1Y_1. Figure 5 shows that angle $\hat{\varphi}$ provides the orientation of the H-plane (measured from the X_1 axis), while $\hat{\alpha}$ indicates the flexion of the ca-

ble. Their values are obtained as:

$$\begin{array}{ll} \textit{flexion angle} & \hat{\alpha} = \sqrt{\hat{\alpha}_y^2 + \hat{\alpha}_x^2} \\ \textit{orientation angle} & \hat{\varphi} = \arctan 2\,(-\hat{\alpha}_x, \hat{\alpha}_y) \end{array}$$

The orientation and flexion angles of the PBA with respect to the global frame are then given as

$$\begin{cases} \varphi = \arctan 2\,(\hat{\alpha}_x, \hat{\alpha}_y) \\ \alpha = \dfrac{b}{b_g} \sqrt{\dfrac{(\hat{\alpha}_y)^2}{\left(1 + \hat{\alpha}_y \dfrac{d}{b_g}\right)^2} + (\hat{\alpha}_x)^2} \end{cases}$$

where b is the PBA span, b_g the goniometer length and d is the offset placement of the goniometer along the X-axis (Figure 2 and 3). The deflection angle θ (defined as the angle subtended between the tip and the base of the PBA) is $\theta = \alpha/2$.

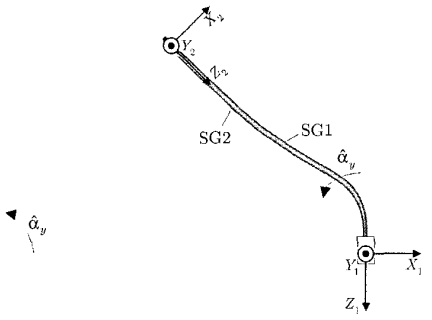

Figure 4 – Biplanar goniometer working principle.

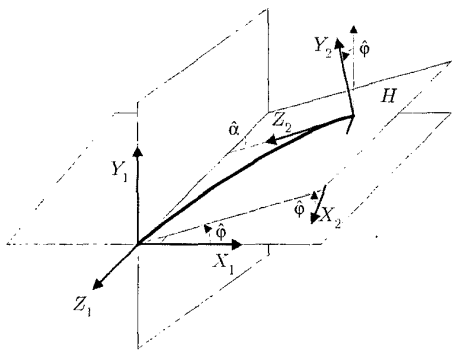

Figure 5 – Measurement in the no-twist condition.

VI. Fin Actuator Description

The fin actuator consists of eight equally spaced PBAs arranged in a series along a mounting rail (Figure 7). Overall length is $L = 1\,\text{m}$. The PBAs bend to act in a similar manner to the fin rays and are interconnected by an elastic material, acting as the fish fin membrane. The membrane currently used has been fabricated from a single sheet of two-way stretch Lycra, folded in half with a "pouch" created for each fin ray.

The fin actuator is attached to a support frame via two sensors measuring the forces generated from the undulations (Figure 6). Each sensor is a thin-walled aluminium pillar with a total of 12 strain gauges attached to its outer cylinder surface. The gauges are arranged in five bridge circuits to provide tri-axial force measurement. Two half bridges measure bending strain on the x- and y-axes, while a full bridge measures the axial load along the sensor.

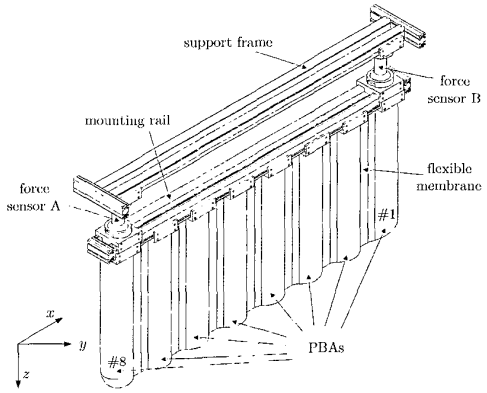

Figure 6 – Fin actuator diagramm.

VII. Results

The fin actuator, coupled to the software used to drive it, allows for the movement of the eight fin rays to be individually controlled, in order to form the desired propulsive wave. This provides a large number of possible propulsive motions (subject to the limitations of the PBAs). As a first approach, and in conjunction with the assumptions of ebt, we have considered sinusoidal variations of the deflection angle, whereby the fin rays oscillate with a (common) frequency f, in the plane lateral to the fin actuator main axis. Furthermore, the amplitude envelope and phase difference p between consecutive PBA units, remain constant. This formulation of the reference PBA trajectories $\mathbf{T}_i$ provides an approximation to the model used in the modified ebt:

$$\mathbf{T}_i(f, \theta_{r0}, \Delta p) = \begin{bmatrix} \varphi_r(t) \\ \alpha_r(t) \end{bmatrix}_i = \begin{bmatrix} \pi/2 \\ 2\theta_{r0} \sin\left(2\pi f t - ip\right) \end{bmatrix}$$

for $i = 0..7$, and where θ_{r0} is the reference maximum deflection angle. The wavelength of the propulsive wave is then $\lambda = 2\pi L/7p$, while its propagation velocity is $V = \lambda f$. With the fin actuator mounted in the tank, measurements were performed to determine the movement characteristics and generated forces, for a range of f, θ_{r0}, and p values. Results presented here are limited to $\theta_{r0} = 23°$, since performance was consistent for all θ_{r0} tested. The maximum deflection angles θ_0 measured for a specific PBA (situated at the middle of the device) are shown in Figure 8a. A complex response has been recorded, indicating the extend and significance of the interactions between the fin actuator and the water in the tank.

The reaction force $\vec{F}$ exerted by the water to the device during undulations is measured by the force sensors and analysed into its Cartesian components F_x, F_y and F_z (see Figure 6). Results for F_x^{ave} (average value) are shown in Figure 8b. The fin actuator is successful in generating thrust that can be reversed, by changing the propagation direction of the propulsive wave (i.e. for $p < 0$). Values of F_x^{ave} up to about 1.5 N are calculated. Absolute thrust force can be seen to increase with p for $|p| < 60°$.

Elongated body theory (modified to take into account the shape of the deflected fin rays) provides a theoretical upper limit for the average propulsive momentum imparted to the water along the x-axis, obtained as

$$M_{x0} = \pi^2 \rho \theta_0 f b^3 \left(R_M \frac{f \sin \psi_{av}}{8} + 0.53 \theta_0 b \cos^3 \psi_{av} \right)$$

where ρ is the density of the water and ψ_{av} is the average angle of momentum shedding, calculated as

$$\sin \psi_{av} = \frac{\int_0^b \left(1 + \frac{b^2}{\kappa^2 m^4}\right)^{-1} dm}{\int_0^b \left(1 + \frac{b^2}{\kappa^2 m^4}\right)^{-1/2} dm}$$

The momentum reduction factor R_M is defined as

$$R_M = \tfrac{1}{2}(1 + R_A)$$

where R_A is the reduction of swept area, resulting from the flexible nature of the fin rays, compared to the case of rigid units oscillating, for the same deflection angle θ_0. It can be shown to equal

$$R_A = \left(\sin 2\theta_0 + 2\theta_0 \cos 2\theta_0 - 4\theta_0 + 4\theta_0^2 \,\text{Si}\, 2\theta_0\right) / 4\theta_0^3$$

where Si is the sine integral. Using the deflection angle measurements of Figure 8a, the theoretical predictions are shown in Figure 8d. Estimations for $\overline{M_x}$, obtained from the experimental F_x data are shown in Figure 8c.

Due to the symmetrical movement of the oscillating fin rays, the average value of F_y was found to be close to zero for the great majority of the test runs. The maximum instantaneous values of $|F_y|$ (denoted as $F_y^{\max}$) are also of interest (Figure 8e). For every combination of f and θ_0, the maximum occurs in the area $-10° \leq p \leq 10°$, as it represents the case where the rays oscillate more or less in phase. As $|p|$ is increased, $F_y^{\max}$ is reduced quite sharply, reflecting the progressive cancellation of sideforces, that occurs as the wavelength is increased. A local minima is reached in the area $40° \leq |p| \leq 50°$, that approximates the condition for which $L/\lambda = 1$. This is in accordance to theoretical and intuitive predictions, since sideforces are more adequately cancelled out for an integer number of wavelengths present across the undulating fin. Accordingly, as $|p|$ is further increased, higher $F_y^{\max}$ values are generated.

Force generation along the z-axis is independent of the waveform propagation direction, as the response is generally symmetrical about the $p = 0$ axis (Figure 8f). Response for F_z^{ave} was generally consistent for all the frequencies tested (apart from $f = 0.95$ Hz), whereby F_z^{ave} is initially negative, and increases gradually, assuming positive values for $|p| > 20°$. A local maximum appears in the region $40° \leq |p| \leq 60°$. The response is differentiated, rather abruptly, for $f = 0.95$ Hz: for $|p| \leq 20°$, the average force is positive, then reverses direction for $30° \leq |p| < 50°$ approximately. As $|p|$ is further increased, F_z^{ave} once again assumes positive values.

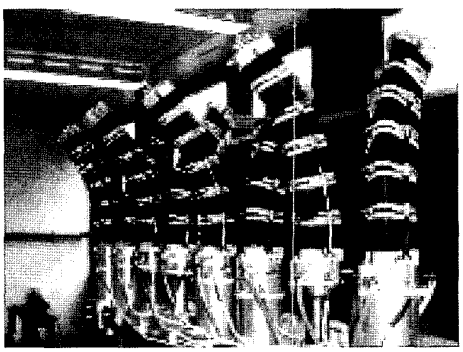

Figure 7 – Array of PBAs forming the fin actuator.

VIII. Conclusions

These preliminary results demonstrated the ability of the fin actuator to generate reversible thrust, pro-

viding data on the relation between the generated forces and the propulsive wave parameters. The modified elongated body theory appears to be a useful analytical tool for estimating the propulsive momentum. Future research will concentrate on alternative propulsive waveforms (including three dimensional movements of the fin rays), improving the membrane design and implementing closed-loop position control of the fin rays. Better testing facilities (a flow channel or drag tank), will permit more comprehensive tests, across a range of relative velocities imposed between the fin actuator and the fluid. Scaling issues necessary to produce adequate force for given underwater vehicle sizes are also being considered. Finally, a hydraulic version of the device, benefiting from increased bandwidth, accuracy and bending ability is planned.

IX. Acknowledgments

This work formed part of the FL.A.P.S. (FLexible Appendage for Positioning and Stabilisation) research program, funded by the UK Engineering and Physical Sciences Research Council, through the Centre for Marine and Petroleum Technology (research grant reference GR/L29217). The authors wish to acknowledge and thank Mr. Bryan Deacon for his help in the mechanical design of the test rig.

References

[1] J. J. Videler. *Fish Swimming.* Chapman and Hall, London, 1993.

[2] M. Sfakiotakis, D. M. Lane, and J. B. C. Davies. Review of fish swimming modes for aquatic locomotion. *IEEE Journal of Oceanic Engineering*, 24(2):237–252, 1999.

[3] D. S. Barrett, M. S. Triantafyllou, D. K. P. Yue, M. A. Grosenbaugh, and M. J. Wolfgang. Drag reduction in fish-like locomotion. *Journal of Fluid Mechanics*, 392:183–212, 1999.

[4] J. M. Kumph, M. S. Triantafyllou, D. Nugent, and M. Santos. Fast-starting and maneuvering vehicles: Robopike and robomuskie. In *Proc. 11th Int. Symp. Unmanned Untethered Submersible Tech.*, pages 439–445, Durham, USA, 1999.

[5] N. Kato. Hydrodynamic characteristics of a mechanical pectoral fin. *Journal of Fluids Engineering-Transactions of the Asme*, 121(3):605–613, 1999.

[6] B. Hobson, M. Murray, and C. A. Pell. Pilotfish: Maximizing agility in an unmanned-underwater vehicle. In *Proc. 11th Int. Symp. Unmanned Untethered Submersible Tech.*, pages 41–51, Durham, USA, 1999.

[7] M. J. Lighthill and R. W. Blake. Biofluiddynamics of balistiform and gymnotiform locomotion. 1. biological background, and analysis by elongated-body theory. *Journal of Fluid Mechanics*, 212(MAR):183–207, 1990.

[8] R. W. Blake. On balistiform locomotion. *Journal of the Marine Biological Association of the United Kingdom*, 58:73–80, 1978.

[9] C. M. Breder and H. E. Edgerton. An analysis of the locomotion of the seahorse, hippocampus hudsonius, by means of high speed cinematography. *Annals of the New York Academy of Sciences*, 43:145–172, 1942.

[10] R. W. Blake. On seahorse locomotion. *Journal of the Marine Biological Association of the United Kingdom*, 56:939–949, 1976.

[11] R. W. Blake. Median and paired fin propulsion. In P. W. Webb and D. Weihs, editors, *Fish Biomechanics*, pages 214–247. Praeger Publishers, New York, 1983.

[12] T. L. Daniel. Forward flapping flight from flexible fins. *Canadian Journal of Zoology-Journal Canadien De Zoologie*, 66(3):630–638, 1988.

[13] G. Robinson and J. B. C. Davies. The parallel bellows actuator. In *Proc. Robotica '98*, pages 195–200, Brasov, Romania, 1998.

[14] J. B. C. Davies, D. M. Lane, G. C. Robinson, D. J. Obrien, M. Pickett, M. Sfakiotakis, and B. Deacon. Subsea applications of continuum robots. In *Proc. International Symposium on Underwater Technology*, pages 363–369, Tokyo, Japan, 1998.

[15] J. B. C. Davies. *A Flexible Three Dimensional Motion Generator.* PhD thesis, Heriot-Watt University, 1996.

[16] F. Casolo and G. Legnani. Choice and measurement of angular variables for biomechanic 3d analysis and simulation, discussion of results collected by a commercial system. In *1st World Congress of Biomechanics*, San Diego, USA, 1990.

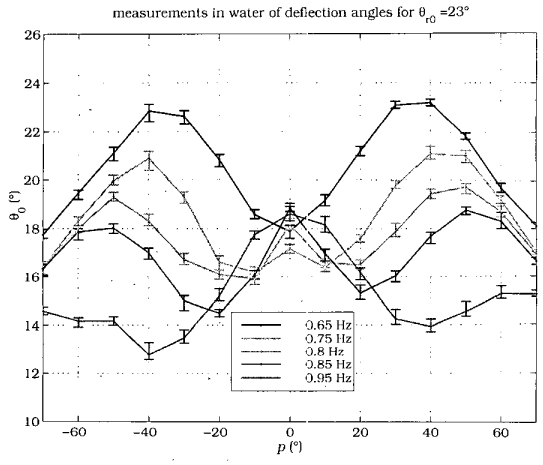

(a) Maximum deflection angles

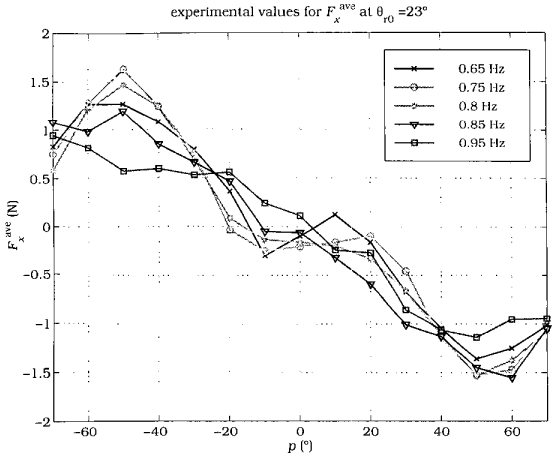

(b) Average thrust forces

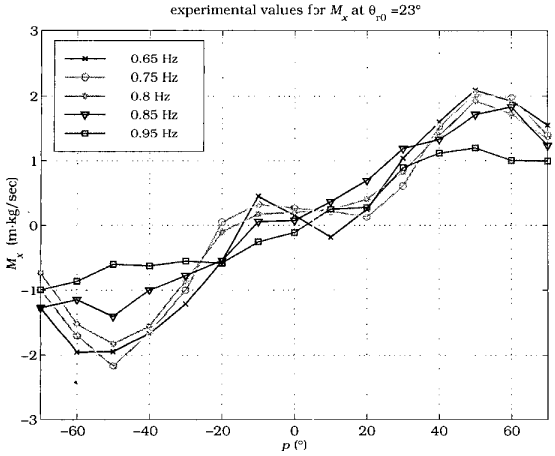

(c) Experimental values for propulsive momentum

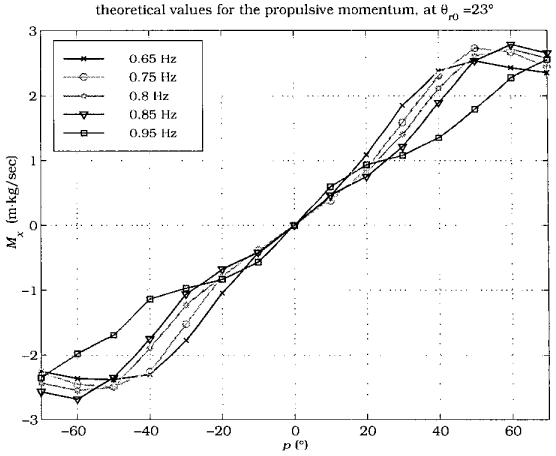

(d) Theoretical estimations for propulsive momentum

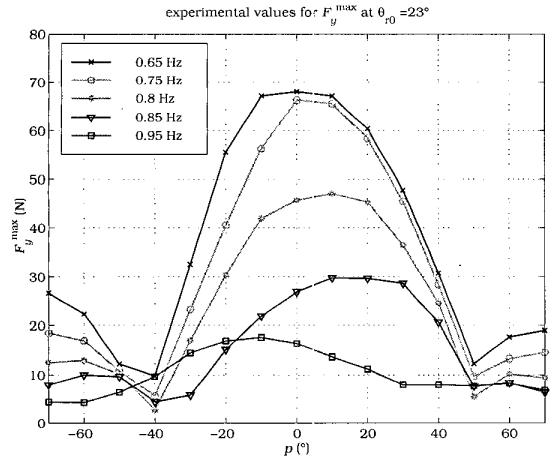

(e) Maximum instanteneous lateral forces

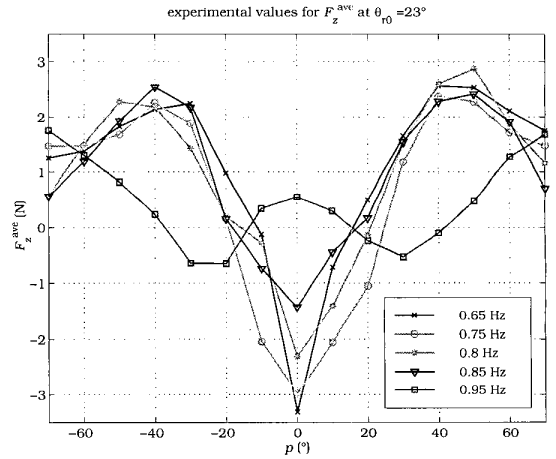

(f) Average forces along the z axis

Figure 8 – Fin actuator test results.